Direct Release of Sombrero-Shaped Magnetite Nanoparticles via Nanoimprint Lithography

*Byung Seok Kwon, Wei Zhang, Zheng Li, and Kannan M. Krishnan**

Magnetic nanoparticles exhibit high potential for biological and biomedical applications,[1–4] ranging from magnetic particle imaging (MPI),[5] to direct drug delivery and hyperthermia[6] as well as stem-cell tracking and gene therapy.[7] For successful in vivo applications, magnetic nanoparticles must be bio-compatible, imposing conditions other than magnetic properties on materials selection. Most of the conventionally used ferromagnetic materials demonstrating high saturation magnetization (Co, Ni, Fe, and their alloys) are cytotoxic due to their oxidation state, or solubility. However, Fe_3O_4, magnetite, demonstrates sufficiently adequate magnetic properties with biocompatibility.[1] Magnetite nanoparticles, in spherical form, are superparamagnetic for sub-100 nm sizes[8–11] for a measurement time of 100 s. Larger particles, >100 nm in diameter, tend to be ferrimagnetic and agglomerate at room temperature due to dipolar coupling. However, for multilayered elements consisting of alternating layers of Fe_3O_4 and Ti, the magneto-static interactions between the layers of the heterostructure will lead to antiparallel orientation of the magnetization in the layers and in the ideal case, effectively cancel their magnetization giving zero remanence. Thus, these synthetic antiferromagnets (SAF) can be fabricated in much larger sizes providing the principal motivations for fabricating and releasing heterostructured elements.[12]

To fabricate magnetite nanoparticles, different chemical methods have been developed.[13–17] These processes are "bottom-up" chemical synthesis methods that enable larger scale production, but they demonstrate critical difficulties of controlling the shape, size, structure, and defects in particles larger than ≈30 nm in size. These difficulties can be overcome by, "top-down" fabrication of magnetic nanoparticles by lithographic methods such as nanoimprint lithography initially developed to directly pattern the resist using a mold.[18–20] Hu et al. further reinforced and combined this particular technique with lift-off and release to fabricate aqueous-stable synthetic antiferromagnetic (SAF) nanoparticles.[21,22] These SAFs have distinct advantages over chemically synthesized ones such as higher magnetic moment, homogeneous particle size, and zero remanence over a wide range of particles sizes from tens of nanometers to micrometers. Zhang et al. used ethylene tetrafluoroethylene (ETFE) to create a "working stamp" instead of using a "master" silicon mold for imprinting and demonstrated improved process in terms of defects prevention and direct release. Specifically, this process prevented significant defects being induced from the silicon mold as well as the degradation, with use, of the silicon mold itself.[22] Thus, they were able to achieve direct release of high-quality disk-shaped magnetic nanoparticles in solution using an ETFE "working stamp," bilayer resist lift-off and silicon etching process specifically designed for the release of the nanoparticle.[22] This nanoimprint lithography process, however, was only developed for the release of metal magnetic nanoparticles rather than the more biologically relevant magnetite nanostructures.

Here, we present an optimized fabrication process for complex, sombrero-shaped, magnetite nanoparticles using nanoimprint lithography via an ETFE mold. We modified the nanoimprint lithography process to fabricate magnetite nanoparticles with a diameter of ≈500 nm directly on Si wafer and released them through a dry etching procedure. By using the combination of the ETFE mold, defect free nanoimprint, bilayer lift-off, and dry etching release, we fabricated magnetite nanoparticles with controlled size, shape, structure, and defects. To demonstrate this process, Fe_3O_4/Ti multilayer, sombrero-shaped SAF nanoparticles, potentially useful for molecular imaging and detection,[23] were fabricated and characterized using scanning electron microscopy (SEM) and a quantum design physical property measurement system (PPMS).

The reproducible fabrication of magnetite nanoparticles was carried through several steps: replication of ETFE, fabrication of bilayer resist, nano-imprinting, lift-off, and release in solution (**Figure 1**). We followed the recipe used by Zhang et al., but adjusted it for magnetite lift-off.[22] To replicate ETFE mold from silicon master mold, we cleaned and ultra-sonicated a sheet of ETFE (DuPont Tefzel) with acetone and isopropyl alcohol for 5 min, blow-dried with nitrogen, and placed onto a clean Si-wafer. The Si master mold with 350 nm holes in a hexagonal lattice, from Lightsmyth Technologies, was placed on the ETFE sheet, then imprinted using a Nanonex NX-B 100 compact thermal nanoimprinter, at 250 °C and 450 psi for 2 min. Next, we spin-coated a bilayer-resist, consisting of LOR 1A (MicroChem) and NXR-1025 (Nanonex), and soft-baked each layer at 200 °C and 150 °C on a hot plate, respectively. After the bilayer-resist was ready, we patterned it with the replicated ETFE mold using Nanonex NX-B100 imprinter (**Figure 2**A). Large area hole arrays (350 nm) of the top layer were obtained. Next, we performed anisotropic oxygen plasma reactive ion etching (RIE) to remove the imprint resist residue, then we

B. S. Kwon, Z. Li, Prof. K. M. Krishnan
Department of Materials Science and Engineering
University of Washington
Seattle, WA 98195, USA
E-mail: kannanmk@uw.edu
Dr. W. Zhang
Argonne National Laboratory
Lemont, IL 60439, USA

DOI: 10.1002/admi.201400511

ADVANCED MATERIALS INTERFACES
www.advmatinterfaces.de

Materials Views
www.MaterialsViews.com

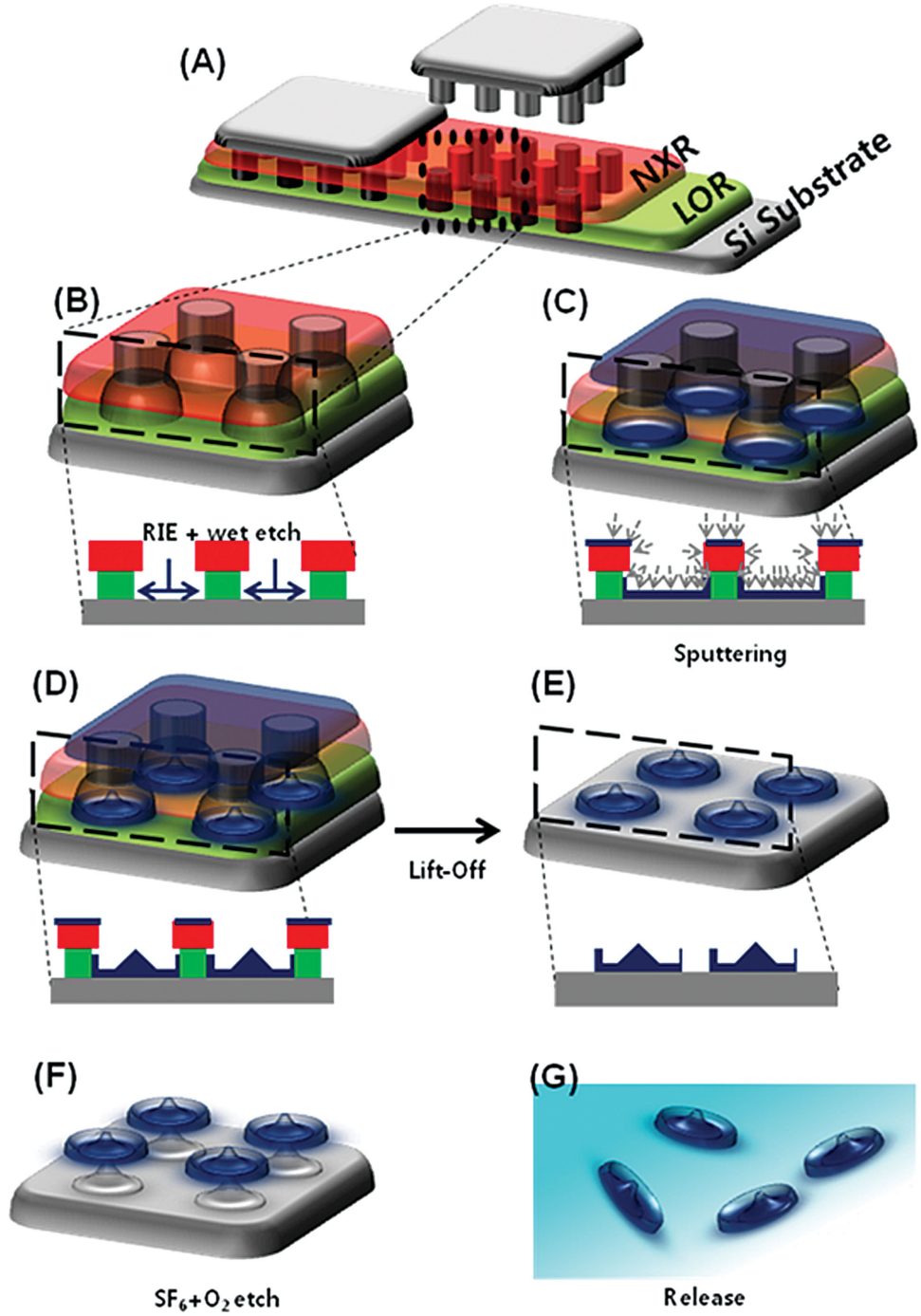

Figure 1. Schematic diagram of nanoimprint process used to fabricate sombrero-shaped magnetic nanoparticles.

selectively etched LOR 1A layer of the patterned bilayer resist to create an undercut. Then, we deposited Fe_3O_4/Ti multilayers using magnetron sputtering under a deposition pressure less than 7.0 mTorr, and at room temperature. Figure 2C–E demonstrate how Fe_3O_4/Ti multilayers are fabricated from a thin sheet to sombrero-shaped particles. Initially, magnetron sputtering deposits materials only at the bottom and with a negligible amount on side-walls, but as deposition time increases, side wall deposition starts to develop significantly. After certain time of deposition (≈2 h), the side-wall is well-defined and is an integral part of sombrero shaped nanoparticles. These sombrero shaped nanoparticles are larger (≈500 nm) in size than the size of the stamp (≈350 nm) because the nondirectional sputtering deposits under the undercut resist profile and even at side-walls (Figure 2C,D). After the deposition, subsequent lift-off removed the bilayer resist and the surplus metals on top to leave

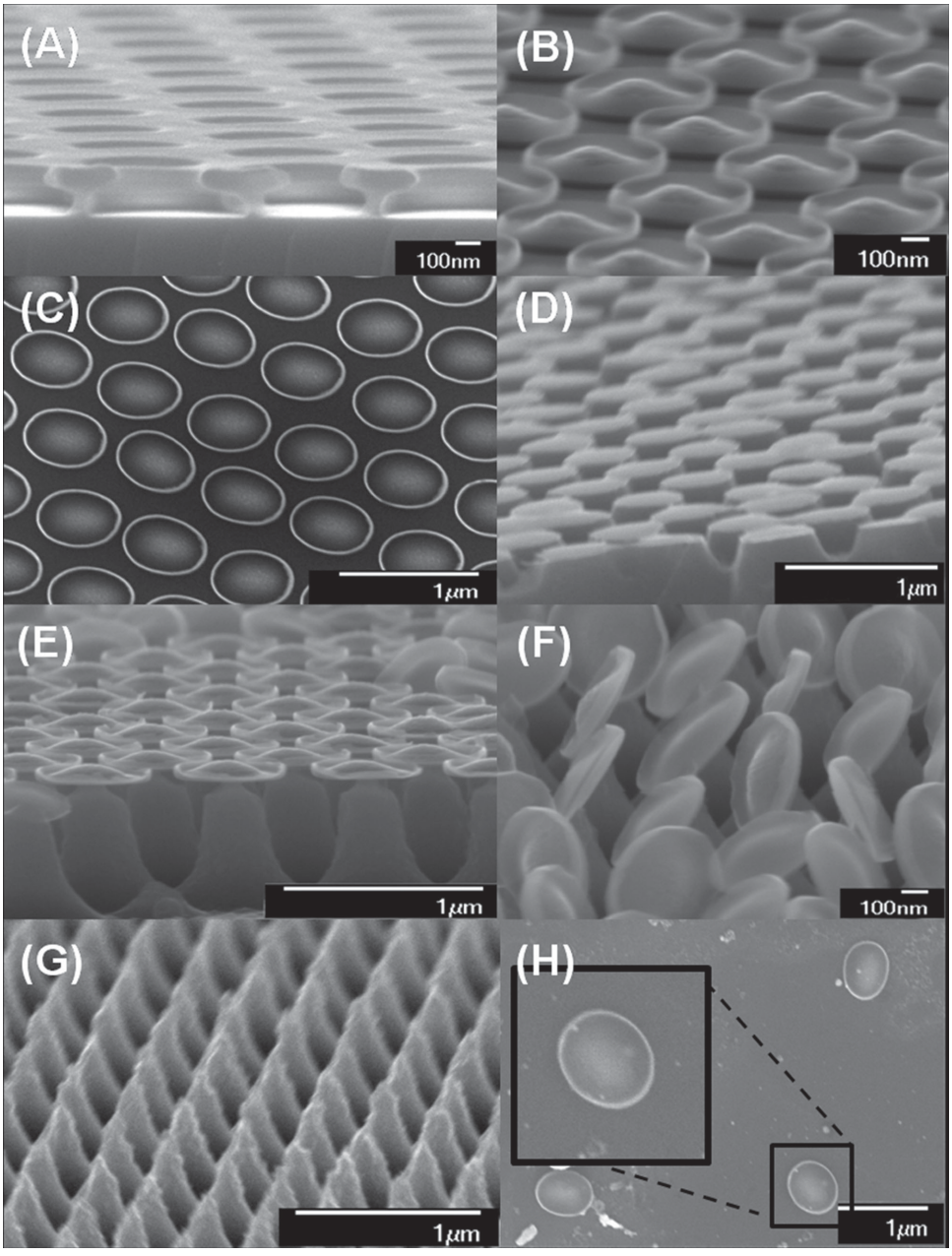

Figure 2. SEM images showing individual steps in the fabrication and release of sombrero-shaped SAF magnetite nanoparticles: A) double resist undercut profile, B,C) array of SAF sombrero-shaped nanoparticles, D–F) SF_6+O_2 etching process to release the nanoparticles, G) silicon substrate after the release, H) nanoparticles after release.

sombrero-shaped magnetite nanoparticles on the silicon substrate (Figure 2F). Finally, using a SF_6 + O_2 mixed gas plasma RIE, the silicon substrate was selectively etched into sharp peaks using the SAF nanoparticles themselves as the etching mask, eventually leaving the SAF magnetite nanoparticles loosely attached to each silicon peak via Van der Waals forces (Figure 2G). Then these magnetite nanoparticles were released by putting the silicon substrate into DI water, followed by a brief ultra-sonication to shake off the nanoparticles (Figure 2H). Finally, these magnetite nanoparticles were characterized with SEM and PPMS to analyze their morphology and magnetic properties.

Each of the steps presented above is demonstrated visually by SEM images. Figure 2A shows the bilayer resist undercut profile after the nanoimprinting and wet etching development. To fabricate the sombrero-shape without defects on the wall, we controlled the time of wet etching in order to develop an undercut profile without any bottom tail; bottom tail refers to undercut resist residue due to under-etch and has to be avoided as it can cause breakage of the side wall at the time of wet etching and

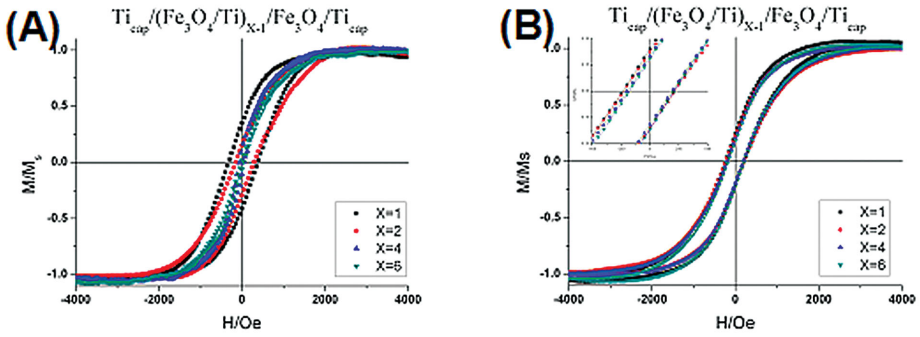

Figure 3. Hysteresis loops of the SAF multilayered nanoparticles measured in the in-plane direction, in which $H_c \approx 0$ is observed at $X = 4$, and $X = 6$, (A) and out-of-plane direction (B) on substrate with different number of alternating layers ($X = 1$, $X = 2$, $X = 4$, $X = 6$).

ultra-sonication. Detail of the relationship between the bottom tail and etching is discussed in an earlier work.[24] Figure 2B,C presents cross-sectional and overhead views, respectively, of arrays of magnetite nanoparticles on a silicon substrate after the lift-off step. The diameter of the sombrero-shaped SAF nanoparticle is ≈500 nm. Our innovation here is to fabricate sombrero-shaped SAF nanoparticle by using nondirectional deposition with bilayer undercut profile. Figure 2D presents intermediate step of $SF_6 + O_2$ etch which shows that the nanoparticles are still attached to Si pillars. Figure 2E,F exhibits the ideal etch result where sombrero-shaped nanoparticles are loosely attached to cone-shaped Si pillars via Van der Waals force. Figure 2E shows that the sombrero-shaped nanoparticles are attached as arrays; however, after slight external force such as slight sudden tilt, they are tilted and only loosely attached to the Si substrate.[22] We tested the etching parameters for releasing the nanoparticles and found that the optimized etching power is 50 W (Trion RIE) with 3 min etching, which is sufficient to fully detach the nanoparticles from the Si wafer. The sombrero-shaped SAF nanoparticles are then released from the original substrate (Figure 2G), and transferred to solution (Figure 2H). The thickness of the center of SAF nanoparticles and diameter of SAF nanoparticles were ≈70 nm, and ≈500 nm respectively, and the height of the side-wall was ≈50 nm which remained intact and unchanged throughout the process of release. Figure 2E,F,H shows the sombrero-shaped SAF nanoparticles transferred without change in shape, structure, and size. Even the thin side-wall was not damaged throughout the process.

To demonstrate the magnetic properties of our SAF, we prepared Fe_3O_4/Ti multilayer elements. There have been many previous papers on synthetic antiferromagnetic (SAF) nanoparticles discussing the variation of magnetic properties with the thickness of each layers.[21–24] We used two sequences of multilayers $Ti/(Fe_3O_4/Ti)_{X-1}/Fe_3O_4/Ti$, with $X = 1$, 2, 4 and 6, deposited by magnetron sputtering. The hysteresis loop measured in the in-plane and out-of-plane directions of the as-fabricated SAFs are shown in **Figure 3**A,B. As the number of ferrimagnetic layers increases from $X = 1$ to $X = 6$, significant decrease of coercivity, H_c, in the in-plane direction, from ≈355 Oe to ≈ < 25 Oe, was observed. This significant decrease of coercivity, H_c, in the in-plane direction was also observed in the micromagnetic simulation of the magnetic reversal of the nanoparticle. Especially, for SAF nanoparticles with $X = 4$, and $X = 6$, near superparamagnet-like behavior ($H_c \approx 0$) was observed which will lead to minimal agglomeration when released into solution and enhance their potential use in biomedical applications. This superparamagnet-like behavior of SAF nanoparticles with biferromagnetic layer in the in-plane direction is consistent with other reports that were previously published.[21–23,25] However, no change in the coercivity was observed in the out-of-plane direction, which remained at ≈200 Oe. Despite the complex shape, the sombrero-shaped SAF nanoparticles have higher aspect ratio in the in-plane direction than the out-of-plane direction. To first order, the magnetization fraction with direction in-plane (97%) and out-of-plane (3%) can be considered to be proportional to their volume fraction in the sombrero-shaped nanoparticles. Due to their shape anisotropy, these SAF nanoparticles primarily prefer in-plane magnetization. Therefore, we observe significant decrease in coercivity since stronger antiparallel magneto-static compensation forces the in-plane magnetization to remain very small as the number of ferromagnetic layer increases. This is reflected in the different hysteresis loops shown in Figure 3A. Moreover, the sombrero-shaped SAF nanoparticles also favors the magnetization components of the side-walls and at the center peak to be along the out-of-plane magnetization direction. However, this out-of-plane magnetization component is significantly smaller compared to the in-plane magnetization component (97:3) due to the aspect ratio of sombrero-shape of the particle. This is consistent with the higher and unchanging coercivity value shown in Figure 3B.

The magnetization state of sombrero-shaped particles were further investigated by micromagnetic simulation (LLG) as shown in **Figure 4** with color wheel indicating the directions of magnetization shown as an inset in Figure 4A. The following dimensions were used for simulations: the diameter of the nanoelement = 500 nm, the thickness of the ferrimagnetic layer = 20 nm, the thickness of the spacer layer = 5 nm, number of ferrimagnetic layer = 4, number of spacer layer = 3, the thickness of the side wall = 3 nm, the total height of side wall = 150 nm, the base diameter of center peak for sombrero-shaped nanoelement, 97.5 nm. The following magnetic parameters were used for simulation: $M_s = 480$ emu cm^{-3}, exchange stiffness constant, $A = 1.32$ μerg cm^{-1}, magneto-crystalline anisotropy, $K_{mc} = 0$ to simulate the polycrystalline magnetite

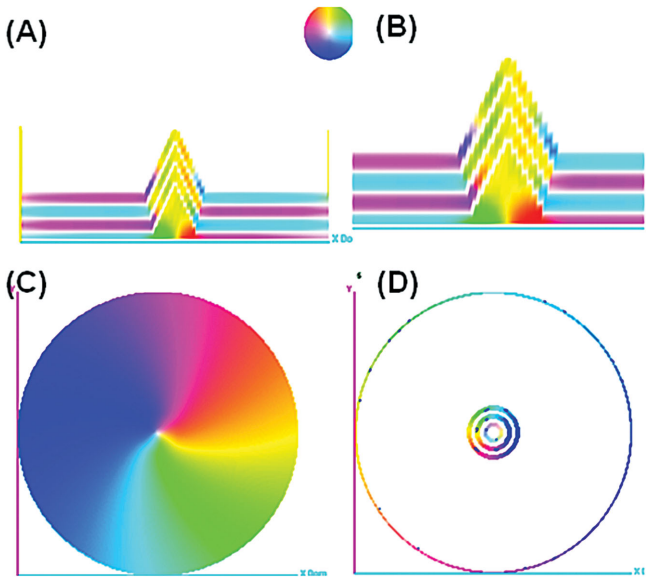

Figure 4. Synthetic antiferromagnetic sombrero-shaped nanoelements used for LLG micromagnetic modeling. For the SAF nanoparticles, alternating layers of ferrimagnetic layers and spacer were used to simulate the mechanism of SAF. Multiple disks with decreasing diameter were used to simulate the central cone. Thin ring at the edge was used to simulate the side wall. A,B) Cross-sectional view of sombrero-shaped nanoelement with an out-of-plane component in the central cone and side wall, anti-parallel magneto-static compensation is shown between layers. C) Domain structures were then simulated at different heights. SAF sombrero-shaped nanoelement shows a single vortex at the bottom layer. However, opposite chirality shows as layer increases due to the antiparallel magneto-static interaction to compensate (D). Finally, inset of (A) is a color wheel which represent the direction of magnetization.

having 2 nm × 2 nm × 25 nm cell. An out-of-plane external field of 5000 Oe was applied and then removed to achieve the remanent state shown in Figure 4A–D. The out-of-plane magnetization direction is shown by taking a side-view slice through the middle of each element. For sombrero-shaped nanoparticles, the LLG simulation predicts a single vortex state in the bottom disk component (Figure 4C) with its magnetic singularity being pinned by the out-of-plane magnetization component of the central cone of the sombrero (Figure 4A). Further, the vortex state of the disk is exchange-coupled to the side-walls (Figure 4D). In addition, antiparallel magneto-static compensation was observed between each ferrimagnetic layers outside the center cone which explains the almost zero coercivity in the in-plane hysteresis loop. In addition, strong out-of-plane magnetization component at side-walls is predicted by the simulation (Figure 4A). In conclusion, the remanent magnetization state of sombrero-shaped nanoparticles is complex and involves both in-plane and out-of-plane components that are consistent with their 3D structures; further, a good agreement was found between magnetic reversal measurements and micromagnetic simulation.

The magnetization state of a single SAF nanoparticle was studied through magnetic force microscopy (MFM). We applied external field higher than the saturation field (≈2500 Oe) parallel to the sample surface and removed the external field to achieve the magnetic remanent state. Then, we investigated magnetic configurations of the particle using 15 nm CoCr coated low moment probes with a lift height of 50 nm.[26] As shown in **Figure 5**, we observed a strong out-of-plane component at both the edge and center of the particles. This is consistent with the hysteresis loop (Figure 3) and micromagnetic simulation (Figure 4). The zero remanent magnetization could possibly be attributed to the anti-parallel magnetostatic compensation between individual ferrimagnetic layers within the sombrero-shaped nanoparticle. This distinct magnetic signal observed through MFM was sensitive to the layer structure of a SAF nanoparticle. To be specific, when the number of Fe_3O_4 and Ti spacer layers double, the magnetic signal under identical imaging conditions becomes much stronger compared to the bilayer-structure where it showed barely any magnetic signal (MFM image of the bilayer-structured particle is not shown here).

To conclude, we have developed a process to fabricate and release the magnetite sombrero-shaped SAF nanoparticles. We used nanoimprint lithography in order to control the size, shape, and structure of these nanoparticles and large volume manufacturing. Our new process suggests a way to improve the quality of conventional SAF nanoparticles by developing a way to fabricate complex sombrero-shaped SAF nanoparticles, which has a superparamagnetic-like behavior and a magnetic structure with both in-plane and out-of-plane magnetization components. This process could potentially enable better functionalization of SAF nanoparticles.

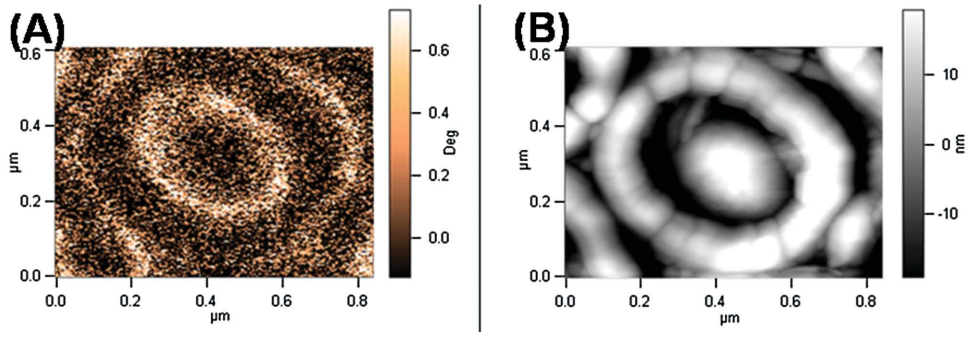

Figure 5. A) Magnetic force microscopy (MFM) image of SAF sombrero-shaped nanoparticles with four alternating Fe_3O_4 layers with a Ti spacer layer between each pair of Fe_3O_4 layers. Out-of-plane component is observed in the central cone and side wall. B) Scanning probe image demonstrates the height profile of same SAF sombrero-shaped nanoparticles scanned in (A) with side-wall and central cone.

ADVANCED MATERIALS INTERFACES
www.advmatinterfaces.de

Acknowledgements

This work was supported by NSF-DMR 1063489. The authors thank Dr. Yufeng Hou and Andrew Lingley for helpful discussions. Nanoimprint work was done at the MFF at the University of Washington.

Received: November 14, 2014
Revised: December 18, 2014
Published online: January 10, 2015

[1] K. M. Krishnan, *IEEE Trans. Magn.* **2010**, *46*, 2523.
[2] A. Fu, W. Hu, L. Xu, R. J. Wilson, H. Yu, S. J. Osterfeld, S. S. Gambhir, S. X. Wang, *Angew. Chem.* **2009**, *121*, 1648.
[3] J.-H. Lee, Y.-M. Huh, Y.-w. Jun, J.-w. Seo, J.-t. Jang, H.-T. Song, S. Kim, E.-J. Cho, H.-G. Yoon, J.-S. Suh, *Nat. Med.* **2006**, *13*, 95.
[4] C. T. Yavuz, J. Mayo, W. Y. William, A. Prakash, J. C. Falkner, S. Yean, L. Cong, H. J. Shipley, A. Kan, M. Tomson, *Science* **2006**, *314*, 964.
[5] R. M. Ferguson, K. R. Minard, A. P. Khandhar, K. M. Krishnan, *Med. Phys.* **2011**, *38*, 1619.
[6] A. P. Khandhar, R. M. Ferguson, J. A. Simon, K. M. Krishnan, *J. Biomed. Mater. Res. A* **2012**, *100*, 728.
[7] M. M. Lin, H.-H. Kim, H. Kim, M. Muhammed, D. K. Kim, *Nano Rev.* **2010**, *1*, 4883.
[8] Z. Liu, Y. Liu, K. Yao, Z. Ding, J. Tao, X. Wang, *J. Mater. Synth. Process.* **2002**, *10*, 83.
[9] M. Winklhofer, K. Fabian, F. Heider, *J. Geophys. Res. Solid Earth* **1997**, *102*, 22695.
[10] A. R. Muxworthy, W. Williams, *J. R. Soc. Interface* **2008**, *06*, 0462.
[11] A. R. Muxworthy, D. J. Dunlop, W. Williams, *J. Geophys. Res. Solid Earth* **2003**, *108*, 2281.
[12] W. Hu, R. J. Wilson, C. M. Earhart, A. L. Koh, R. Sinclair, S. X. Wang, *J. Appl. Phys.* **2009**, *105*, 7B508.
[13] I. Martínez-Mera, M. Espinosa-Pesqueira, R. Pérez-Hernández, J. Arenas-Alatorre, *Mater. Lett.* **2007**, *61*, 4447.
[14] R. Massart, *IEEE Trans. Magn.* **1981**, *17*, 1247.
[15] S. Sun, H. Zeng, *J. Am. Chem. Soc.* **2002**, *124*, 8204.
[16] J. Baumgartner, A. Dey, P. H. Bomans, C. Le Coadou, P. Fratzl, N. A. Sommerdijk, D. Faivre, *Nat. Mater.* **2013**, *12*, 310.
[17] J. Baumgartner, L. Bertinetti, M. Widdrat, A. M. Hirt, D. Faivre, *PloS one.* **2013**, *8*, e57070.
[18] S. Y. Chou, P. R. Krauss, P. J. Renstrom, *J. Vac. Sci. Technol., B: Microelectron. Nanometer Struct.–Process., Meas., Phenom.* **1996**, *14*, 4129.
[19] W. Zhang, K. M. Krishnan, *J. Micromech. Microeng.* **2014**, *24*, 093001.
[20] S. Y. Chou, P. R. Krauss, P. J. Renstrom, *Science* **1996**, *272*, 85.
[21] W. Hu, R. J. Wilson, A. Koh, A. Fu, A. Z. Faranesh, C. M. Earhart, S. J. Osterfeld, S. J. Han, L. Xu, S. Guccione, *Adv. Mater.* **2008**, *20*, 1479.
[22] W. Zhang, K. M. Krishnan, *J. Appl. Phys.* **2012**, *111*, 07B509.
[23] J. S. Wi, E. S. Barnard, R. J. Wilson, M. Zhang, M. Tang, M. L. Brongersma, S. X. Wang, *ACS Nano* **2011**, *5*, 6449
[24] W. Zhang, D. Weiss, K. M. Krishnan, *J. Micromech. Microeng.* **2011**, *21*, 045024.
[25] W. Zhang, M. E. Bowden, K. M. Krishnan, *J. Appl. Phys.* **2013**, *113*, 17B502.
[26] Z. Li, K. M. Krishnan, *J. Appl. Phys.* **2013**, *113*, 17B901.